ELSEVIER

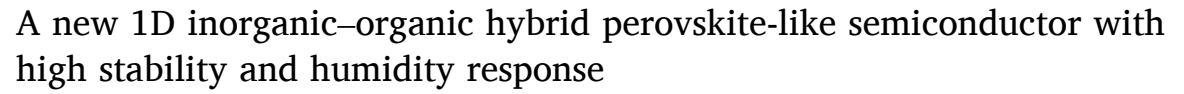
Contents lists available at ScienceDirect

# **Inorganic Chemistry Communications**

journal homepage: www.elsevier.com/locate/inoche



### Short communication





- <sup>a</sup> College of Chemistry, Fuzhou University, Fuzhou City, Fujian Province 350116, PR China
- b State Key Laboratory of Structural Chemistry, Fujian Institute of Research on the Structure of Matter, Chinese Academy of Sciences, Fuzhou, Fujian 350002, PR China
- <sup>c</sup> University of Chinese Academy of Sciences, Beijing 100049, China
- <sup>d</sup> Fujian Science & Technology Innovation Laboratory for Optoelectronic Information of China, Fuzhou, Fujian 350108, China
- e Key Laboratory of Jiangxi Province for Persistent Pollutants Control and Resources Recycle (Nanchang Hangkong University), Nanchang 330063, China

#### ARTICLE INFO

#### Keywords: Semiconductor Perovskite-like Inorganic-organic hybrid Humidity sensor

#### ABSTRACT

Inorganic-Organic hybrid perovskite-like materials have potential application in photodetection, sensor and solar cells etc. However, these materials still face the challenge of poor stability. A new inorganic–organic hybrid material was synthesized by solvothermal method using  $H_2DAB$  as the template and counter cation. The structure is composed of one-dimensional (1D) inorganic perovskite-like chain,  $[(Me_3)DAB(Me_3)]^{2+}$  (DAB = benzidine) dications and water molecules. This compound exhibits good stability to water and organic solvents, and shows typical semiconductor behavior. Interestingly, the compound also shows great potential for humidity sensing, including linear sensitivity (10–100%), high response (5 orders of magnitude of current change), and fast recovery time.

# 1. Introduction

Hybrid inorganic–organic perovskite-like material have been extensively studied in the fields of ferroelectric [1,2], catalysts [3,4], sensing [5], and optics [6–10]. The perovskite-like structure with similar octahedral coordination environment as perovskite structure but richer connection mode makes it highly structural designable [11,12]. Moreover, they exhibit similar performance as perovskite materials [13–19]. However, these perovskite-like materials also encounter stability problems [20–22]. Many methods have been exploited to improve the stability, such as encapsulated [23,24] and doped [25–27] etc. However, these post-modification methods will cause the problem of increased costs, and it is still urgent to develop simple strategies to improve the stability of such materials.

Low-dimensional inorganic—organic hybrid materials tend to show better moisture resistance than three-dimensional hybrid semiconductor materials, which may be benefited by the connection model of the inorganic structure [28–31]. In one-dimensional inorganic—organic hybrid materials, the inorganic chains are separated by organic cations, which effectively prevent the entry of water molecules [11]. In addition,

the low-dimensional structure can confine the electrons in the nanowires or layers to facilitate their transmission [32], thus exhibiting good electrical properties for FET [33], photodetection [34–36] etc. Therefore, the creation of perovskites-like material with one-dimensional infinite extension chain would exhibit excellent electronic properties without compromising the stability aspects.

Here, we synthesized a new 1D hybrid perovskite-like material  $[(Me_3)DAB(Me_3)]PbI_4\cdot H_2O$  (1) by a simple one-step hydrothermal method, which is consisted by 1D inorganic  $PbI_4^-$  anion chains and  $H_2DAB$  cations. Compound 1 shows excellent stability in various polar molecules and aqueous solutions. In addition, this compound also exhibits typical semiconductor properties and is highly sensitive to humidity, demonstrating its potential application for humidity sensing.

### 2. Experimental section

# 2.1. Material

Lead(II) iodide (PbI<sub>2</sub>), benzidine (DAB), hydroiodic Acid (HI), and methanol (MeOH) were purchased from Adamas-beta. All solvents and

E-mail address: gewang@fjirsm.ac.cn (G.-E. Wang).



<sup>\*</sup> Corresponding author at: State Key Laboratory of Structural Chemistry, Fujian Institute of Research on the Structure of Matter, Chinese Academy of Sciences, Fuzhou, Fujian 350002, PR China.

reagents were purchased without further purification.

#### 2.2. Synthesis of compound 1

 $PbI_2$  (0.165 g) and DAB (0.092 g) were mixed with methanol (5 mL), and concentrated HI (1 mL, 45%) were added at room temperature, and then the mixture was packaged in a 25 mL Teflon-lined reaction vessel and heated at 130 °C for 2 days. After slowly cooling to room temperature, orange block crystals 1 were found in 81% yield (based on PbI<sub>2</sub>), which were designated as [(Me<sub>3</sub>)DAB(Me<sub>3</sub>)]PbI<sub>4</sub>·H<sub>2</sub>O by single crystal X-ray diffraction. The crystal is mechanically separated from the powder and cleaned with ethanol. Elem. Anal. Calcd. For [(Me<sub>3</sub>)DAB(Me<sub>3</sub>)] PbI<sub>4</sub>·H<sub>2</sub>O (%): C: 21.55, H: 2.81, N:2.79. Found: C: 21.32, H: 2.78, N: 2.75.

#### 2.3. Single crystal X-ray crystallography

The single crystal diffraction data of compound 1 was collected on a Rigaku Ultra-Saturn 70 diffractometer with graphite-monochromatic Mo- $K_{\alpha}$  radiation ( $\lambda=0.71073$  Å), and the intensity data set was collected using  $\omega$  scanning technology, and the  $\mathit{Lp}$  effect was corrected. The initial crystal structure was solved by Olexsys Olex2 1.2 package of crystallography software using the intrinsic phase method and refined by the full matrix method based on  $\mathit{F}^2$ . Anisotropy was applied to all nonhydrogen atoms, and hydrogen atoms on carbon and nitrogen were geometrically generated. The crystallographic data details of compound 1 are provided in Table 1, and the bond distance and angle are shown in Table 2 and Table 3, respectively. The crystallographic data of compound 1 is stored in the Cambridge Crystallographic Data Center with CCDC 2060017. These data can be downloaded free of charge from the Cambridge Crystallography Data Center at www.ccdc.cam.ac.uk/data request/cif.

# 2.4. Characterization methods

The Powder X-ray diffraction (PXRD) of samples were recorded on a Rigaku Miniflex 600 diffractometer (Cu K $\alpha$ ,  $\lambda=1.540598$  Å). The simulation curve of [(Me<sub>3</sub>)DAB(Me<sub>3</sub>)]PbI<sub>4</sub>·H<sub>2</sub>O is calculated and fitted by Mercury Version 1.4 software. Thermogravimetric analysis (TGA) was carried out using NETZSCHSTA449C under nitrogen atmosphere. Ultraviolet–Visible diffuse reflectance spectra (DRS) were measured on a

Table 1
Crystal data and structural refinement detail of 1.

Crystal data	1
Formula	C18H28N2OPbI4
Color and habit	orange block
Crystal system	Orthorhombic
Space group	Pnma
A/Å	18.4554(19)
b/Å	16.3455(17)
c/Å	19.1611(17)
$\alpha/^{\circ}$	90
$\beta/^{\circ}$	90
γ/°	90
$V/\mathrm{\AA}^3$	5780.2(10)
Z	8
Formula weight	1001.20
$ ho_{ m calcd}/{ m g~cm}^{-3}$	2.301
$\mu/\mathrm{mm}^{-1}$	10.119
F(000)	3600.0
$\theta$ (°)	6.992 to 51.998
Completeness	99.51%
Independent reflections ( $R_{int}$ )	5871 [ $R_{int} = 0.0730$ , $R_{sigma} = 0.0319$ ]
Reflections measured	55,654
$T_{\min}$ , $T_{\max}$	0.47558,1.000
$R_1$ , $wR_2$ indices (obs.)	$R_1 = 0.0596, wR_2 = 0.1588$
$R_1$ , wR <sub>2</sub> indices (all data)	$R_1 = 0.0932, wR_2 = 0.1912$
GOF on $F^2$	1.131

Table 2
Selected bond lengths (Å) for 1.

Pb1-I1	3.260(1)	Pb1-I2	3.356(2)
Pb1-I3	3.130(2)	Pb1-I4	3.302(1)
Pb1-I5	3.340(2)	Pb1-I6	3.107(1)

Table 3
Selected bond angles (°) for 1.

I1-Pb1-I2	93.10(4)	I1-Pb1-I3	92.24(3)
I1-Pb1-I4	175.27(3)	I1-Pb1-I5	92.51(2)
I1-Pb1-I6	89.08(3)	I2-Pb1-I3	96.85(5)
I2-Pb1-I4	82.85(4)	I2-Pb1-I5	80.09(4)
I2-Pb1-I6	170.70(4)	I3-Pb1-I4	90.68(4)
I3-Pb1-I5	174.48(4)	I3-Pb1-I6	92.08(4)
I4-Pb1-I5	84.40(3)	I4-Pb1-I6	94.54(4)
I5-Pb1-I6	90.79(4)		

Lamda 950 (Perkin<br/>Elmer, USA) in 200–800 nm range using  ${\rm BaSO_4}$  as a contrast background.

# 2.5. Conductivity measurement

Single crystal of 1 is placed on the quartz glass, and then sticks two gold wires (diameter 50  $\mu$ m) on both sides of the crystal with silver paste to construct the single crystal device. The single crystal device was placed in a variable temperature oven, and its temperature-dependent I-V curve was recorded by Keithley 4200.

#### 2.6. Humidity sensing measurement

The humidity response measurement of gas sensor was carried out in a self-made device. All tests were performed at room temperature. The suspension of compound 1 is formed by mixing the ground crystal with ethanol. Then the suspension of compound 1 was dropped on the Ag-Pd interdigital electrode by the drop casting method to make the sensor. The device was placed in a quartz tube with a stable gas flow rate (600 mL/min), and the sensor test was performed by switching between dry air and humidity air, and the Keithley 2602B Source meter was used to record the current change (under a bias of 1 V).

#### 3. Results and discussion

### 3.1. Crystal structure analysis

Structural analysis confirmed that compound 1 crystallizes in the orthorhombic system of Pnma space group, which consists of onedimensional (1D) infinite PbI<sub>4</sub> chain, [(Me<sub>3</sub>)DAB(Me<sub>3</sub>)]<sup>2+</sup> dications and water molecules. Each lead atom coordinates with six iodine atoms to form an octahedral configuration (Fig. 1a). This PbI<sub>6</sub> octahedron is the basic configuration of the perovskite-like structure, and forms the perovskite-like anion module through a variety of connection methods. The Pb-I bond distance is 3.107(1)-3.356(2) Å, which is within the normal bond length range. Two PbI<sub>6</sub> octahedra face-sharing with each other to form a dinuclear cluster, and this dinuclear cluster further linked to a 1D perovskites-like chain through corner-sharing mode (Fig. 1b). The 1D inorganic chain extends along b axis with a width of 10.247(1) Å (Fig. S1). The  $[(Me_3)DAB(Me_3)]^{2+}$  cations are alternately stacked with each other in a crisscross pattern along the b axis. Four alternately stacked cationic chains form a one-dimensional channel along b axis, and the  $PbI_4^-$  anion chain is cleverly encapsulated in this channel and surrounded by cations (Fig. 1c). The closest distance between two adjacent  $[(Me_3)DAB(Me_3)]^{2+}$  cations is 4.328(3) Å, which is triflely larger than standard  $\pi \cdots \pi$  stacking distance (3.8 Å), indicating that there is no  $\pi \cdot \pi$  stacking interaction (Fig. S2). The distance of the shortest I-C bond (3.604(23) Å) between (PbI<sub>4</sub>)<sup>2-</sup> and [(Me<sub>3</sub>)DAB

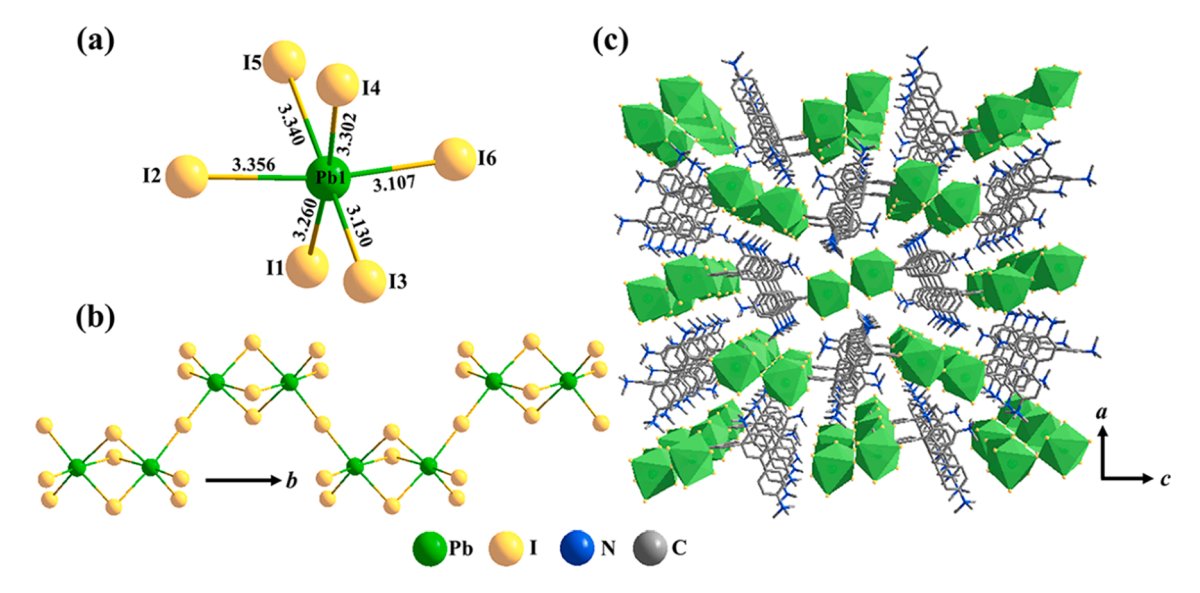


Fig. 1. (a) The PbI<sub>6</sub> octahedron. (b) 1D chain structure of 1 composed of PbI<sub>6</sub> octahedron. (c) The PbI<sub>4</sub>- anion chains are filled in channels formed by cation stacked along the b axis (the hydrogen atoms and oxygen atoms are omitted for clarity).

 $(Me_3)]^{2+}$  cation are smaller than the sum of their ion diameters. Water molecules are filled in the structural space, the nearest I···O distance is 5.013(20) Å, indicates that there is no halogen bond interaction between PbI<sub>4</sub> and water molecules (Fig. S3).

Organic cations are cleverly distributed around the conductive 1D inorganic chains, and methyl from the organic cations are exposed at the outermost periphery of the cation channel, which is likely to promote the water stability of the material [37,38]. Notable, this type of material can be designed to transform its physical properties by designing cations [14]. For example, by choosing the appropriate size of the cation to design the dimensions of the material or using hydrophobic cations to fill the surrounding 1D chains to improve moisture resistance [39,40].

# 3.2. Experimental stability

To further study the chemical stability of compound 1, single crystals were immersed in water and various organic solvents (e.g. MeOH, HI and  $CH_3CN$ , etc) for two hour. PXRD indicated that compound 1 can preserve good crystallinity in these solvents without any change, indicating that it has good chemical stability (Fig. 2a). In addition, the

optical pictures before and after immersion in the aqueous solution also show that the crystals have not been changed (Fig. 2b, c). Thermogravimetric (TG) analysis shows that compound 1 loses weight at 200 °C and 550 °C under the flow rate of N<sub>2</sub> (Fig. 3b). Notable, compound 1 also remains stable at 200 °C, indicating the outstanding stability of 1.

#### 3.3. Experimental band gap

The band gap of compound  $\mathbf{1}$  was studied by ultraviolet–visible diffuse reflectance spectroscopy (Fig. 3a). The optical band gap of  $\mathbf{1}$  is calculated by the Kubelka-Munk formula to be 2.4 eV (see supporting information for details), indicating that compound  $\mathbf{1}$  is a potential semiconductor material.

# 3.4. Variable temperature electronic conductivity

To further study the semiconductor characteristics of compound  ${\bf 1}$ , the two-terminal direct current method was used to measure the conductivity of compound  ${\bf 1}$  with different temperature. The relationship between the current and temperature of compound  ${\bf 1}$  single crystal was

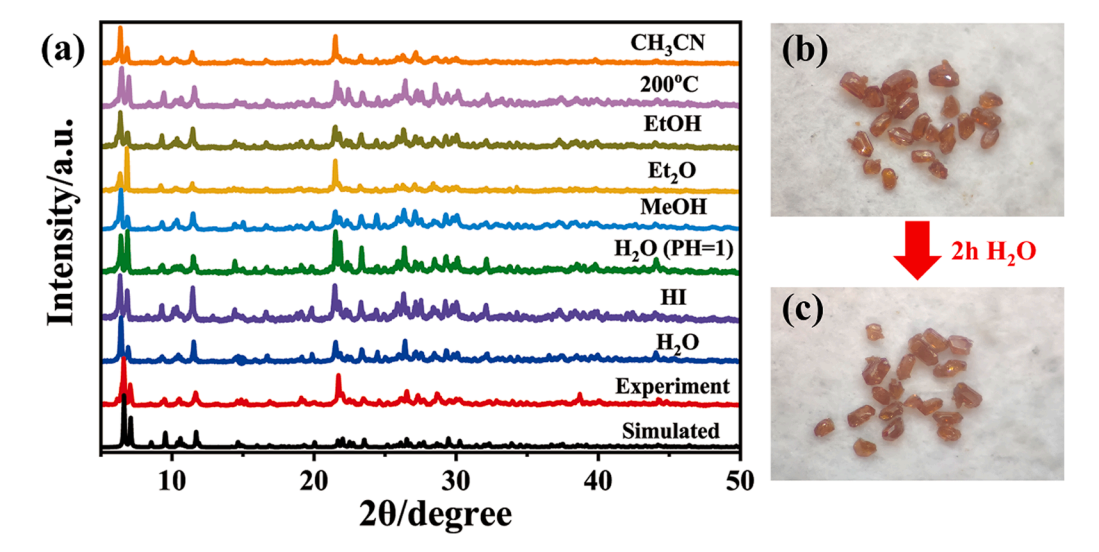


Fig. 2. (a) PXRD of compound 1 after incubating in different solutions (Hydroiodic, acetonitrile water and methanol etc) for 2 h at room temperature. (b) Optical picture of compound 1 before soaking in water.

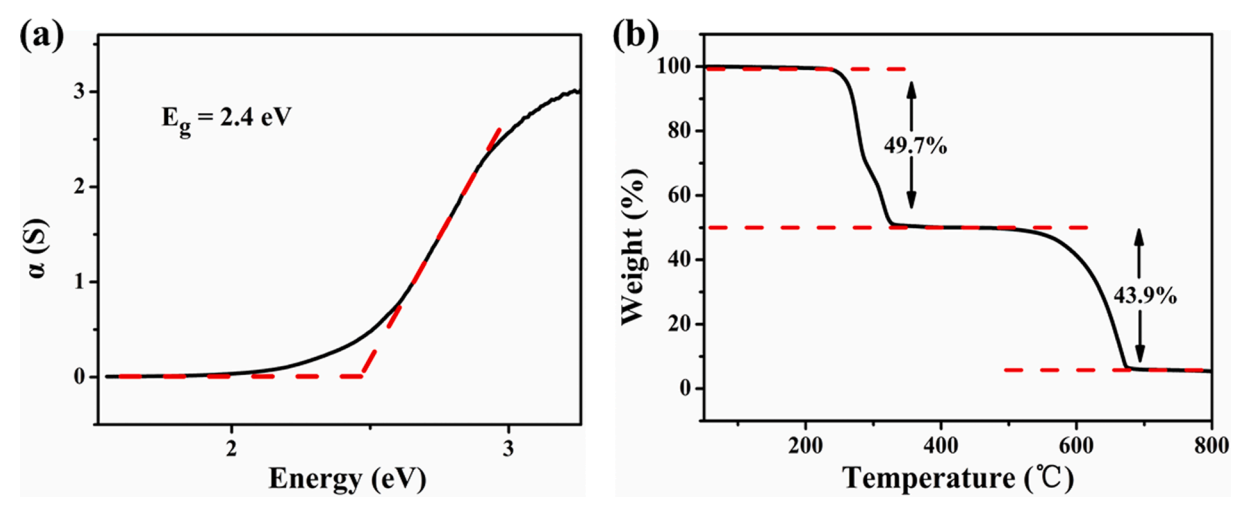


Fig 3. (a) Optical absorption spectrum for 1. (b) TG curve of 1 under N<sub>2</sub> flow.

shown in Fig. 4a. By increasing the temperature from 30 °C to 120 °C, the conductivity of single crystal 1 increased from  $9.6 \times 10^{-10} \, \mathrm{S \ cm^{-1}}$  to  $2.65 \times 10^{-7} \, \mathrm{S \ cm^{-1}}$  (Fig. S4). The phenomenon of the conductivity increases with the increase of temperature further indicates 1 has the typical semiconducting property. The relationship between the logarithm of conductivity ( $Ln \, \sigma$ ) and the reciprocal of temperature (1000/T) at different temperatures is shown in Fig. 4b. According to Arrhenius equation, the activation energy (Ea) of compound 1 can be calculated to be  $0.647 \, \mathrm{eV}$ .

# 3.5. Humidity sensor

Humidity is the most common physical quantity used to express the content of water vapor in the air. It is still a challenge to prepare a high-performance humidity sensor [41]. Inspired by the excellent stability of compound 1, the humidity test of compound 1 was carried out using the previously reported home-made gas sensing system at room temperature [42]. The sensor is placed in a closed quartz tube to maintain a stable voltage (1 V) in a dry air atmosphere, and switch between dry air and humid air to observe changes in current. Each relative humidity concentration requires 10 min of bubbling to reach saturated water vapor. The switching time of dry/humid air is 10 min/5 min respectively. The real-time dynamic response curve of compound 1 based sensor under different humidity is shown in Fig. 5a. The result shows that compound

1 has outstanding response at different humidity concentrations. When humid air enters the test chamber, the current of the sensor rapidly increases and reaches the saturation value. Immediately after the sensor was exposed to dry air again, the current quickly dropped to the initial position. Compound 1 not only showed a response of 5 orders of magnitude under 100% humidity, but also had a response under 10% low humidity, which fully demonstrated that compound 1 has excellent humidity-sensitive ability. To judge the performance level of compound 1 more conveniently, we set the ratio of humidity air current ( $I_{humidity}$ ) to dry air current ( $I_{dry}$ ) as the humidity response value:

$$R_{response} = I_{humidity}/I_{dry} - 1 = R_{dry}/R_{humidity} - 1$$
 (1)

After calculating the response value under different humidity, the response value of 10–100% humidity was plotted on the logarithm diagram of response concentration (Fig. 5b), and the data showed a good linear relationship in the range of 10% – 100% RH. The response of a single cycle (RH = 90%) is normalized to evaluate the response recovery level of compound 1, the response time ( $t_{resonse}$ ) is set to 90% of the maximum current value and the recovery time ( $t_{recovery}$ ) are calculated to be 3.6 min and 42 s, respectively (Fig. S5). Notably, the recovery time is shorter than response time in each humidity cycle test. This is probably due to the non-porous structure of compound 1, and the water adsorption/desorption behavior occurs on the surface of the material, which

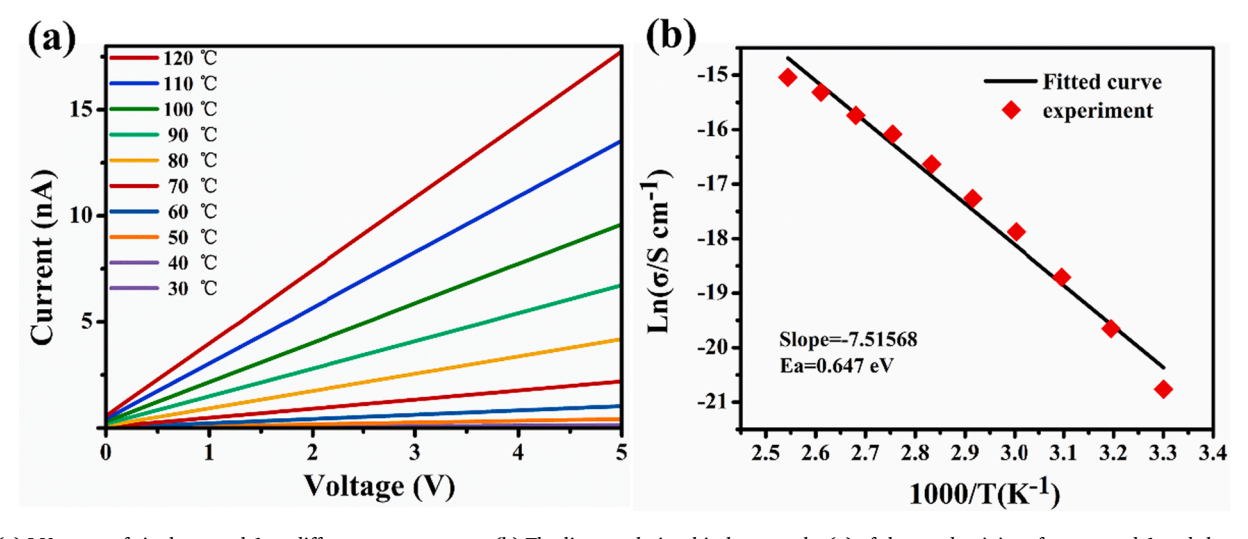
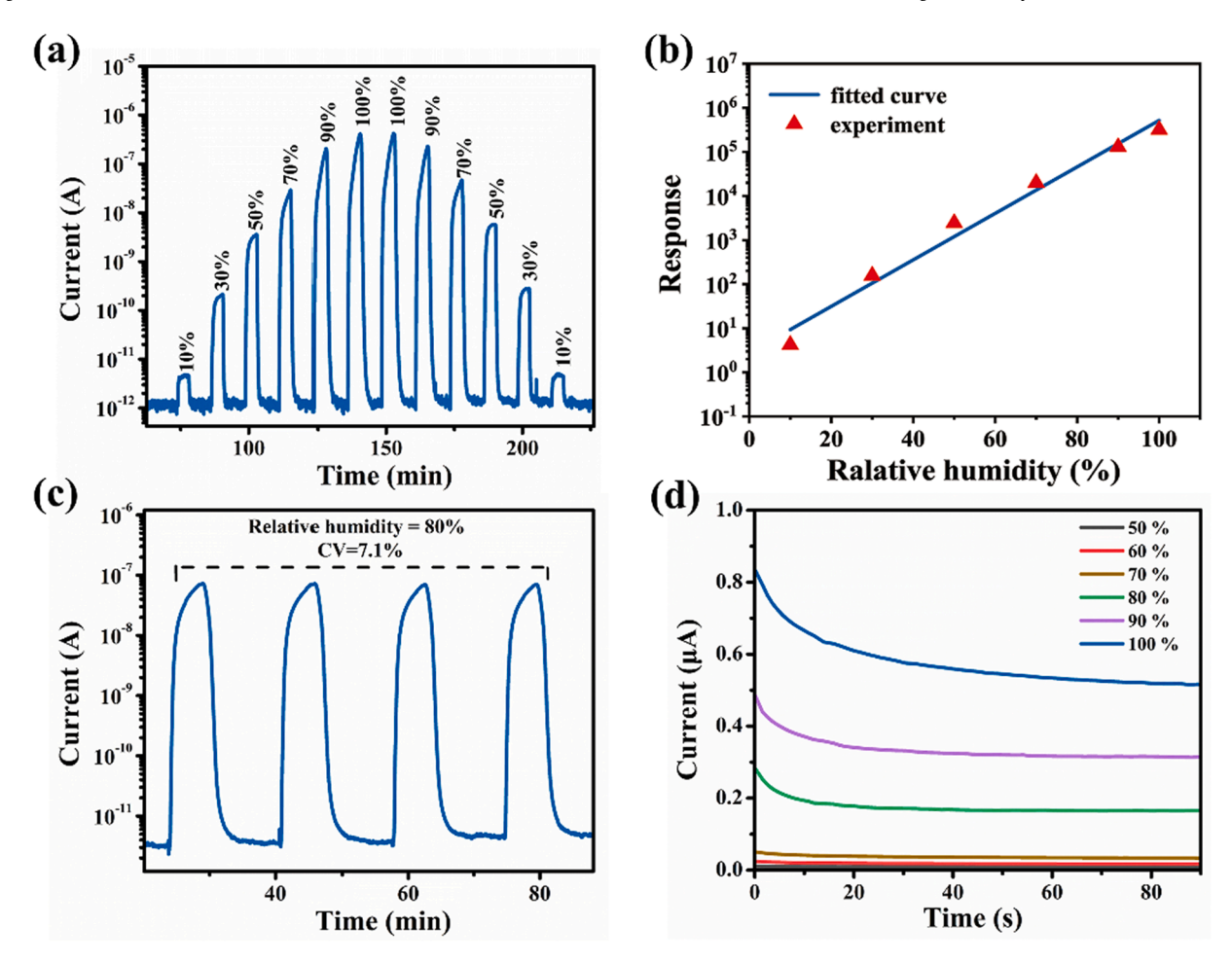


Fig. 4. (a) I-V curve of single crystal 1 at different temperatures. (b) The linear relationship between  $\ln(\sigma)$  of the conductivity of compound 1 and the reciprocal temperature.



**Fig. 5.** Humidity sensing performance of **1** based device. (a) Response of **1** to different relative humidity at room temperature. (b) Linear fitting curve of response and relative humidity of **1.** (c) The stability of compound **1** at 80% humidity for **4** cycles. (d) Instantaneous polarity reversal curve of **1** under different humidity.

makes the  $H_2O$  molecules easier to transfer, resulting in a rapid recovery rate. To further study the cycle stability of 1 based humidity sensor, we use the coefficient of variation (CV) as a reference, which is defined as:

$$CV = R_{SD}/R_{average} \times 100\% \tag{2}$$

where  $R_{SD}$  is the standard deviation (SD) of responses, and  $R_{average}$  is the average response value of cycles at same RH condition. As shown in Fig. 5c, 4 cycles of testing were carried out in 80% humidity atmosphere. The CV value of the compound 1 based sensor was calculated to be 7.1%, which shows that it has good cycle stability. All data show that this sensor has great potential in the field of humidity detection.

# 3.6. Humidity sensing mechanism

The explanation of the mechanism of humidity sensing has always been a difficult problem, and most studies have focused on surface conduction as the mechanism of humidity sensing [43,44]. In order to further investigate whether water molecules conduct through the surface of the material, here, the humidity mechanism in compound 1 is investigated by means of instantaneous polarity reversal (Fig. 5d). The instantaneous polarity reversal is to observe the change of current by switching between positive and negative DC voltages to determine the cause of the change in moisture-induced conductivity [45,46]. To prevent the electrolysis of water, we used a voltage of 1 V for the instantaneous polarity reversal test. Under different RH, the current of compound 1 gradually decay and tends to be stable when the instantaneous positive voltage is applied. The decayed current reflects the two stages of conductivity change. When compound 1 was applied with a

positive voltage, the initial current (ionic conduction) dominated the change in conductivity, but as the current in the ionic conduction phase continues to decay, electronic conduction gradually replaces ionic conduction to stabilize the current. This indicates that the humidity-sensitive response of compound 1 is likely to be dominated by electronic conduction. The decrease in resistance may be due to the fact that the water molecules and hydroxyl functional groups between the surface of the sensing material and electrode reduce the activation energy and barrier of the material [41].

#### 4. Conclusions

In conclusion, we successfully synthesized a one-dimensional perovskite-like inorganic–organic hybrid material  $[(Me_3)DAB(Me_3)]$  PbI $_4\cdot H_2O$ , which has an infinite 1D chain structure. The compound 1 has good stability in various solutions, and can maintain high crystallinity under water atmosphere. The optical band gap measured by ultraviolet diffuse reflection is 2.4 eV. The conductivity of compound 1 increases with the temperature, showing typical semiconductor characteristics. In addition, the humidity sensor of this material has a good linear response at 10–100% relative humidity, and a response of 5 orders magnitude high at 100% relative humidity, showing great potential for humidity sensor.

### **Declaration of Competing Interest**

The authors declare that they have no known competing financial interests or personal relationships that could have appeared to influence

the work reported in this paper.

#### Acknowledgement

This work was supported by the National Natural Science Foundation of China (21822109, 2020000052, 21905280, 21975254, 21950410532, 24074283), Key Research Program of Frontier Science, CAS (QYZDB-SSW-SLH023), International Partnership Program of CAS (121835KYSB201800), the Natural Science Foundation of Fujian Province (2017J05094), China Post-doctoral Science Foundation (2019M662254), and the Youth Innovation Promotion Association CAS (2018342), Key Laboratory of Jiangxi Province for Persistent Pollutants Control and Resources Recycle Open Research Fund (ES202080085).

#### Appendix A. Supplementary data

Supplementary data to this article can be found online at https://doi. org/10.1016/j.inoche.2021.108581.

#### References

- [1] Z. Sun, A. Zeb, S. Liu, C. Ji, T. Khan, L. Li, M. Hong, J. Luo, Exploring a lead-free semiconducting hybrid ferroelectric with a zero-dimensional perovskite-like structure, Angew. Chem. Int. Ed. 55 (2016) 11854–11858.
- [2] M. Ksiądzyna, A. Gągor, A. Piecha-Bisiorek, A. Ciżman, W. Medycki, R. Jakubas, Exploring a hybrid ferroelectric with a 1-D perovskite-like structure: bis (pyrrolidinium) pentachloroantimonate(iii), J. Mater. Chem. C 7 (2019) 10360–10370.
- [3] V.V. Voytovich, S.A. Kurnosenko, O.I. Silyukov, I.A. Rodionov, I.A. Minich, I. A. Zvereva, Study of n-alkylamine intercalated layered perovskite-like niobates HCa<sub>2</sub>Nb<sub>3</sub>O<sub>10</sub> as photocatalysts for hydrogen production from an aqueous solution of methanol, Front. Chem. 8 (2020) 300.
- [4] G.N. Liu, R.Y. Zhao, B. Xu, Y. Sun, X.M. Jiang, X. Hu, C. Li, Design, synthesis, and photocatalytic application of moisture-stable hybrid lead-free perovskite, ACS Appl. Mater. Interfaces 12 (2020) 54694–54702.
- [5] J.M. Bermudez-Garcia, M. Sanchez-Andujar, S. Yanez-Vilar, S. Castro-Garcia, R. Artiaga, J. Lopez-Beceiro, L. Botana, A. Alegria, M.A. Senaris-Rodriguez, Role of temperature and pressure on the multisensitive multiferroic dicyanamide framework [TPrA][Mn(dca)<sub>3</sub>] with perovskite-like structure, Inorg. Chem. 54 (2015) 11680–11687.
- [6] A.N. Usoltsev, M. Elshobaki, S.A. Adonin, L.A. Frolova, T. Derzhavskaya, P. A. Abramov, D.V. Anokhin, I.V. Korolkov, S.Y. Luchkin, N.N. Dremova, K. J. Stevenson, M.N. Sokolov, V.P. Fedin, P.A. Troshin, Polymeric iodobismuthates [Bi3I10] and [Bi14] with N-heterocyclic cations: promising perovskite-like photoactive materials for electronic devices, J. Mater. Chem. A 7 (2019) 5057-5066
- [7] C. Peng, X. Song, J. Yin, G. Zhang, H. Fei, Intrinsic white-light-emitting metalorganic frameworks with structurally deformable secondary building units, Angew. Chem. Int. Ed. 58 (2019) 7818–7822.
- [8] G.E. Wang, G. Xu, M.S. Wang, L.Z. Cai, W.H. Li, G.C. Guo, Semiconductive 3-D haloplumbate framework hybrids with high color rendering index white-light emission, Chem. Sci. 6 (2015) 7222–7226.
- [9] G.E. Wang, X.M. Jiang, M.J. Zhang, H.F. Chen, B.W. Liu, M.S. Wang, G.C. Guo, Crystal structures and optical properties of iodoplumbates hybrids templated by in situ synthesized 1,4-diazabicyclo[2.2.2]octane derivatives, CrystEngComm 15 (2013).
- [10] Z. Wang, Q. Dan, R.-Y. Zhao, R.-D. Xu, G.-N. Liu, C. Li, Optical properties of two bismuth(III) halide hybrids with pyridyl sulfide derivative counter cations, Inorg. Chem. Commun. 111 (2020) 107632.
- [11] Z. Song, J. Zhao, Q. Liu, Luminescent perovskites: recent advances in theory and experiments, Inorg. Chem. Front. 6 (2019) 2969–3011.
- [12] B. Saparov, D.B. Mitzi, Organic-inorganic perovskites: structural versatility for functional materials design, Chem. Rev. 116 (2016) 4558–4596.
- [13] Q. Li, S. Li, K. Wang, Z. Quan, Y. Meng, B. Zou, High-pressure study of perovskite-like organometal halide: band-gap narrowing and structural evolution of [NH<sub>3</sub>-(CH<sub>2</sub>)<sub>4</sub>-NH<sub>3</sub>]CuCl<sub>4</sub>, J. Phys. Chem. Lett. 8 (2017) 500–506.
- [14] B. Kou, W. Zhang, C. Ji, Z. Wu, S. Zhang, X. Liu, J. Luo, Tunable optical absorption in lead-free perovskite-like hybrids by iodide management, Chem. Commun. 55 (2019) 14174–14177.
- [15] X.L. Song, G.F. Wei, J. Sun, C.D. Peng, J.L. Yin, X. Zhang, Y.L. Jiang, H.H. Fei, Overall photocatalytic water splitting by an organolead iodide crystalline material, Nat. Catal. 3 (2020) 1027–1033.
- [16] Y. Wang, S. Guo, H. Luo, C. Zhou, H. Lin, X. Ma, Q. Hu, M.H. Du, B. Ma, W. Yang, X. Lu, Reaching 90% photoluminescence quantum yield in one-dimensional metal halide C<sub>4</sub>N<sub>2</sub>H<sub>14</sub>PbBr 4 by pressure-suppressed nonradiative loss, J. Am. Chem. Soc. 142 (2020) 16001–16006.
- [17] G.E. Wang, M.S. Wang, M.J. Zhang, L.Z. Cai, B.W. Liu, C.J. Zhang, G.C. Guo, J. S. Huang, Haloplumbate hybrids with organically coordinated halometal complexes as templates and mixed halo atoms: Solvothermal syntheses, crystal structures, and optical properties, Inorg. Chem. Commun. 23 (2012) 137–141.

- [18] G.E. Wang, C. Sun, M.S. Wang, G.C. Guo, Semiconducting crystalline inorganicorganic hybrid metal halide nanochains, Nanoscale 12 (2020) 4771–4789.
- [19] V. Gomez, S. Klyatskaya, O. Fuhr, S. Kalytchuk, R. Zboril, M. Kappes, S. Lebedkin, M. Ruben, Pressure-modulated broadband emission in 2D layered hybrid perovskite-like bromoplumbate, Inorg. Chem. 59 (2020) 12431–12436.
- [20] Z. Li, L. Kong, S. Huang, L. Li, Highly luminescent and ultrastable CsPbBr3 perovskite quantum dots incorporated into a silica/alumina monolith, Angew. Chem. Int. Ed. 56 (2017) 8134–8138.
- [21] W.-J. Xu, Z.-Y. Du, W.-X. Zhang, X.-M. Chen, Structural phase transitions in perovskite compounds based on diatomic or multiatomic bridges, CrystEngComm 18 (2016) 7915–7928.
- [22] G.N. Liu, R.Y. Zhao, R.D. Xu, Q. Liu, B. Xu, Y.Y. Wang, Q. Wu, J.N. Wang, Y. Nie, C. Li, Constructing moisture-stable hybrid lead iodine semiconductors based on hydrogen-bond-free and dual-iodine strategies, J. Mater. Chem. C 7 (2019) 7700–7707
- [23] L.N. Quan, R. Quintero-Bermudez, O. Voznyy, G. Walters, A. Jain, J.Z. Fan, X. Zheng, Z. Yang, E.H. Sargent, Highly emissive green perovskite nanocrystals in a solid state crystalline matrix, Adv. Mater. 29 (2017) 1605945.
- [24] Y. Wei, X. Deng, Z. Xie, X. Cai, S. Liang, P.A. Ma, Z. Hou, Z. Cheng, J. Lin, Enhancing the stability of perovskite quantum dots by encapsulation in crosslinked polystyrene beads via a swelling-shrinking strategy toward superior water resistance, Adv. Funct. Mater. 27 (2017) 1703535.
- [25] Z.J. Yong, S.Q. Guo, J.P. Ma, J.Y. Zhang, Z.Y. Li, Y.M. Chen, B.B. Zhang, Y. Zhou, J. Shu, J.L. Gu, L.R. Zheng, O.M. Bakr, H.T. Sun, Doping-enhanced short-range order of perovskite nanocrystals for near-unity violet luminescence quantum yield, J. Am. Chem. Soc. 140 (2018) 9942–9951.
- [26] X. Zhang, Y. Zhang, X. Zhang, W. Yin, Y. Wang, H. Wang, M. Lu, Z. Li, Z. Gu, W. W. Yu, Yb(3+) and Yb(3+)/Er(3+) doping for near-infrared emission and improved stability of CsPbCl<sub>3</sub> nanocrystals, J. Mater. Chem. C 6 (2018) 10101–10105.
- [27] Y. Zhou, J. Chen, O.M. Bakr, H.-T. Sun, Metal-doped lead halide perovskites: synthesis, properties, and optoelectronic applications, Chem. Mater. 30 (2018) 6589–6613.
- [28] C. Hanmandlu, A. Singh, K.M. Boopathi, C.S. Lai, C.W. Chu, Layered perovskite materials: key solutions for highly efficient and stable perovskite solar cells, Rep. Prog. Phys. 83 (2020) 086502.
- [29] J.K. Pious, A. Katre, C. Muthu, S. Chakraborty, S. Krishna, V.C. Nair, Zero-dimensional lead-free hybrid perovskite-like material with a quantum-well structure, Chem. Mater. 31 (2019) 1941–1945.
- [30] D.H. Cao, C.C. Stoumpos, O.K. Farha, J.T. Hupp, M.G. Kanatzidis, 2D homologous perovskites as light-absorbing materials for solar cell applications, J. Am. Chem. Soc. 137 (2015) 7843–7850.
- [31] I.C. Smith, E.T. Hoke, D. Solis-Ibarra, M.D. McGehee, H.I. Karunadasa, A layered hybrid perovskite solar-cell absorber with enhanced moisture stability, Angew. Chem. Int. Ed. 53 (2014) 11232–11235.
- [32] Z. Yuan, C. Zhou, Y. Tian, Y. Shu, J. Messier, J.C. Wang, L.J. van de Burgt, K. Kountouriotis, Y. Xin, E. Holt, K. Schanze, R. Clark, T. Siegrist, B. Ma, Onedimensional organic lead halide perovskites with efficient bluish white-light emission. Nat. Commun. 8 (2017) 14051.
- [33] G. Zheng, W. Lu, S. Jin, C.M. Lieber, Synthesis and fabrication of high-performance n-type silicon nanowire transistors, Adv. Mater. 16 (2004) 1890–1893.
   [34] H. Song, T. Li, J. Zhang, Y. Zhou, J. Luo, C. Chen, B. Yang, C. Ge, Y. Wu, J. Tang,
- [34] H. Song, T. Li, J. Zhang, Y. Zhou, J. Luo, C. Chen, B. Yang, C. Ge, Y. Wu, J. Tang, Highly anisotropic Sb<sub>2</sub>Se<sub>3</sub> nanosheets: Gentle exfoliation from the bulk precursors possessing 1D crystal structure, Adv. Mater. 29 (2017) 1700441.
- [35] B. Polyakov, B. Daly, J. Prikulis, V. Lisauskas, B. Vengalis, M.A. Morris, J. D. Holmes, D. Erts, High-density arrays of germanium nanowire photoresistors, Adv. Mater. 18 (2006) 1812–1816.
- [36] Z. Wu, C. Ji, S. Wang, W. Zhang, Y. Wang, L. Li, S. Zhao, Z. Sun, J. Luo, (2-Methylpiperidine)PbI<sub>3</sub>: an ABX<sub>3</sub>-type organic-inorganic hybrid chain compound and its semiconducting nanowires with photoconductive properties, J. Mater. Chem. C 5 (2017) 11466–11471.
- [37] H.N. Hoang, T.A. Hill, D.P. Fairlie, Connecting hydrophobic surfaces in cyclic peptides increases membrane permeability, Angew. Chem. Int. Ed. 60 (2020) 1–7.
- [38] W. Iradwikanari, O. Hirohito, K. Maki, N. Anders, Y. Taro, Direct interaction of water ice with hydrophobic methyl-terminated Si(111), J. Phys. Chem. C 114 (2010) 19004–19008.
- [39] Z. Shi, Z. Cao, X. Sun, Y. Jia, D. Li, L. Cavallo, U. Schwingenschlogl, Uncovering the mechanism behind the improved stability of 2D organic-inorganic hybrid perovskites, Small 15 (2019) 1900462.
- [40] F.C. Hanusch, E. Wiesenmayer, E. Mankel, A. Binek, P. Angloher, C. Fraunhofer, N. Giesbrecht, J.M. Feckl, W. Jaegermann, D. Johrendt, T. Bein, P. Docampo, Efficient planar heterojunction perovskite solar cells based on formamidinium lead bromide, J. Phys. Chem. Lett. 5 (2014) 2791–2795.
- [41] X.J. Lv, M.S. Yao, G.E. Wang, Y.Z. Li, G. Xu, A new 3D cupric coordination polymer as chemiresistor humidity sensor: narrow hysteresis, high sensitivity, fast response and recovery, Sci. China Chem. 60 (2017) 1197–1204.
- [42] M.S. Yao, W.X. Tang, G.E. Wang, B. Nath, G. Xu, MOF thin film-coated metal oxide nanowire array: significantly improved chemiresistor sensor performance, Adv. Mater. 28 (2016) 5229–5234.
- [43] C. Sun, K.R.G. Karthik, S.S. Pramana, L.H. Wong, J. Zhang, H. Yizhong, C.H. Sow, N. Mathews, S.G. Mhaisalkar, The role of tin oxide surface defects in determining nanonet FET response to humidity and photoexcitation, J. Mater. Chem. C 2 (2014) 940–945.

- [44] T. Zhang, Y. He, R. Wang, W. Geng, L. Wang, L. Niu, X. Li, Analysis of dc and ac properties of humidity sensor based on polypyrrole materials, Sens. Actuators B Chem. 131 (2008) 687–691.
- [45] K. Jiang, H. Zhao, T. Fei, H. Dou, T. Zhang, A guest/host composite of Fe(NO<sub>3</sub>)<sub>3</sub>/ nanoporous polytriphenylamine assembly for humidity sensor, Sens. Actuators B Chem. 222 (2016) 440–446.
- [46] K. Jiang, T. Fei, F. Jiang, G. Wang, T. Zhang, A dew sensor based on modified carbon black and polyvinyl alcohol composites, Sens. Actuators B Chem. 192 (2014) 658–663.